High-pressure-induced phase transitions in the ferroelectric bis-thiourea pyridinium iodide inclusion compound

2008 J. Phys.: Condens. Matter 20 485222

(http://iopscience.iop.org/0953-8984/20/48/485222)

J. Phys.: Condens. Matter **20** (2008) 485222 (7pp) doi:10.1088/0953-8984/20/48/485222

High-pressure-induced phase transitions in the ferroelectric bis-thiourea pyridinium iodide inclusion compound

P Bilski[1], L Bobrowicz-Sarga[1], P Czarnecki[1], H Małuszyńska[1], I Natkaniec[2,3] and J Wąsicki[1]

[1] Institute of Physics, Adam Mickiewicz University, Umultowska 85, 61-614 Poznań, Poland
[2] Frank Laboratory of Neutrons Physics, JINR, 141980 Dubna, Russia
[3] H Niewodniczański Institute of Nuclear Physics, PAS, Radzikowskiego 152, 31-342 Kraków, Poland

Received 17 June 2008, in final form 10 September 2008
Published 28 October 2008
Online at stacks.iop.org/JPhysCM/20/485222

Abstract
The effect of temperature and pressure on physical properties of the ferroelectric bis-thiourea pyridinium iodide inclusion compound has been studied by dielectric spectroscopy, neutron spectroscopy, neutron powder diffractometry, single crystal x-ray diffraction and nuclear magnetic resonance (NMR). At ambient pressure two structural phase transitions have been revealed: at $T_1 = 161$ K between phases I and II and at $T_2 = 141$ K between phases II and III. Phase III with increasing pressure splits into two phases, IIIa and IIIb. The temperatures of the phase transitions $T_{\mathrm{I–II}}$, $T_{\mathrm{II–IIIa}}$ and $T_{\mathrm{IIIa–IIIb}}$ increase with increasing pressure. The p–T phase diagram constructed for this compound shows two triple points of coordinates 150 K, 100 MPa and 115 K, 100 MPa.

(Some figures in this article are in colour only in the electronic version)

1. Introduction

Interesting physico-chemical properties of inclusion compounds of thiourea with pyridinium salts, in particular the discovery of ferroelectric properties of pyridinium nitrate [1] and iodide [2], have stimulated interest in these systems.

The crystal structure of bis-thiourea pyridinium iodide $(2(CS(NH_2)_2)(C_5H_5NH)^+I^-$, hereafter T_2PyHI) consists of two sublattices. The host lattice is built of ribbons of hydrogen-bonded thiourea molecules and iodide ions. Four ribbons form channels in which the guest lattice built of the pyridinium cations is located (figure 1) [2, 3]. The cations are relatively free to reorient in the channels.

The dynamics of the cation in pyridinium iodide $((C_5H_5NH)^+I^-$, hereafter PyHI) is well recognized both at ambient pressure [4] and at high pressure [5]. This salt undergoes a first order phase transition at 249 K [4], a temperature which is shifted to higher values with increasing pressure. Below this temperature the cation performs reorientations about the axis perpendicular to its plane through inequivalent potential barriers [4, 5]. In the high-temperature phase the cation performs reorientations over equivalent barriers [6, 7].

It is interesting to investigate a high-pressure effect on the physical properties in a much more complex system containing the pyridinium cation like the title compound T_2PyHI.

In the pyridinium salts showing only one phase transition (as in PyHI), no ferroelectric ordering was observed. In the pyridinium salts in which at least two phase transitions are observed and the anion symmetry is tetrahedral (BF_4, ClO_4, ReO_4, IO_4) or pseudotetrahedral (FSO_3, $FCrO_3$), ferroelectric ordering was observed in the intermediate- and/or low-temperature phase [8–13]. As follows from the analysis of spontaneous polarization, these ferroelectrics are mainly of the order–disorder type [14–18].

The inclusion compound of T_2PyHI undergoes two phase transitions (at $T_{\mathrm{I–II}} = 141$ K and $T_{\mathrm{II–III}} = 161$ K) and has ferroelectric properties in the low-temperature phase and in the intermediate phase [2]. The ^{1}H NMR study has shown that the pyridinium cation undergoes reorientations about the axis perpendicular to its plane through inequivalent potential barriers (similarly as in PyHI) [19]. In T_2PyHI not only the pyridine cation has a dipole moment, but the thiourea molecule

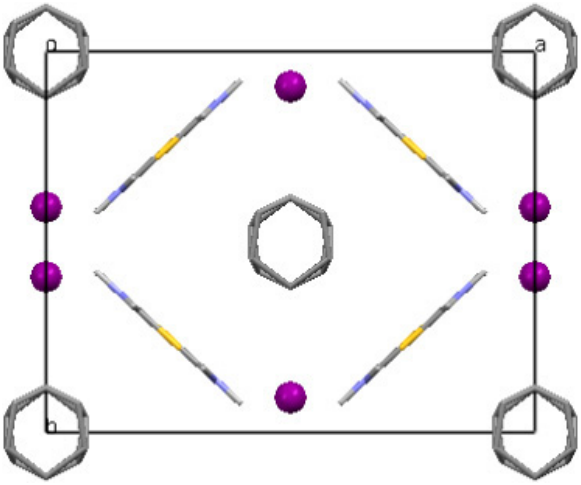

Figure 1. View of the thiourea pyridinium iodide inclusion compound (phase I, $T = 295$ K) along the channel axis. Thiourea forms channels in which cations stack. Anions are at the edge of the channels [2].

as well. The nature of ferroelectricity in this system is not fully known yet.

Important information on the character of the ferroelectricity can be obtained from the p–T phase diagram. To be able to draw the diagram, the phase transitions have been studied by dielectric spectroscopy and nuclear magnetic resonance (NMR). Results obtained by these methods have been supplemented with measurements of elastic and inelastic neutron scattering and single crystal x-ray diffraction.

2. Experimental details

The high-pressure dielectric measurements were performed in a high-pressure chamber connected with a gas compressor GCA-10 (UNIPRESS). The dielectric properties were measured by a Hewlett-Packard 4192A impedance analyser for frequencies ranging from 10 kHz to 13 MHz, at a few values of hydrostatic pressure from 50 to 450 MPa in the temperature range covering the phase transitions. The measuring ac electric field was about 1 V cm^{-1}. The dielectric properties were studied in the pressed polycrystalline pellets with silver electrodes deposited on the surfaces.

The proton spin–lattice relaxation times T_1^{H} for a polycrystalline sample were measured under hydrostatic pressure varied from 0.1 up to 800 MPa in the temperature range 90–300 K. The measuring set-up included a pulsed NMR spectrometer working at 25 MHz, a U-11 (UNIPRESS) helium gas compressor and a beryllium–copper high-pressure cell.

Neutron spectra were measured by the time of flight method on a NERA-PR spectrometer working in inverted geometry [20]. This spectrometer installed at an IBR-2 pulsed reactor at JINR in Dubna, Russia, permitted simultaneous recording of neutron powder diffraction (NPD) spectra and incoherent inelastic neutron scattering (IINS). A polycrystalline sample to be studied at different temperatures was placed in a cryostat cooled by a closed-cycle refrigerator permitting temperature changes from 20 to 350 K, within the

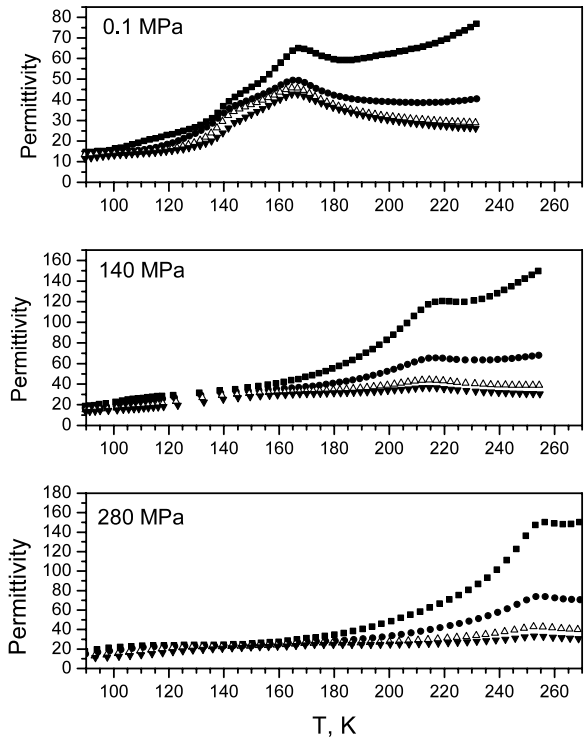

Figure 2. The temperature dependences of the dielectric permittivity for a few frequencies and pressures: ■, 1 kHz; ●, 10 kHz; △, 100 kHz; ▽, 1000 kHz.

accuracy of 0.5 K. Measurements of neutron spectra as a function of hydrostatic pressure were performed on the same spectrometer with the aid of a high-pressure set-up. The high-pressure gaseous helium arrangement consisted of the U11 gas compressor, a high-pressure cell made from aluminium alloy and the cryostat. The high-pressure cell, up to 400 MPa, was connected to a gas compressor by a beryllium–copper capillary and arranged inside a top loaded cryostat cooled by liquid nitrogen with adjustable temperature in the range 90–400 K. This arrangement gives a possibility of carrying out measurements of neutron scattering spectra under pressure conditions which can be kept within the limit of 5 MPa at a stable temperature within the accuracy of 0.5 K [21].

Single crystal x-ray data were collected on a KM-4 diffractometer with a point detector, using Mo Kα radiation, a graphite monochromator and an ω–2θ scan technique. The cycles of cooling and heating were carried out at a rate of 120 K h^{-1} using an Oxford Cryosystem. The temperature dependent cell parameters were obtained by setting angles of 25 reflections in the 15–25° 2θ range and at 18 temperatures from 110 to 290 K.

3. Results

3.1. Dielectric and NMR spectroscopy

The temperature dependences of the dielectric permittivity for a few frequencies and pressures are presented in figure 2. The temperature dependence of dielectric permittivity at ambient pressure reveals two

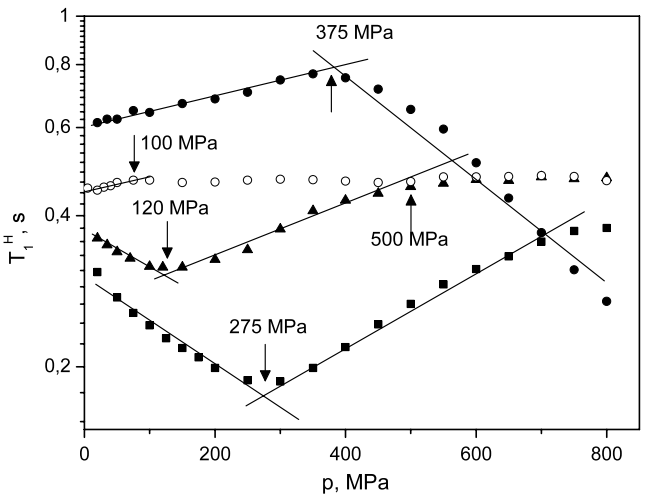

Figure 3. The pressure dependences of the spin–lattice relaxation time T_1^H at a few temperatures: ●, 250 K; ■, 160 K; ▲, 130 K; ○, 100 K.

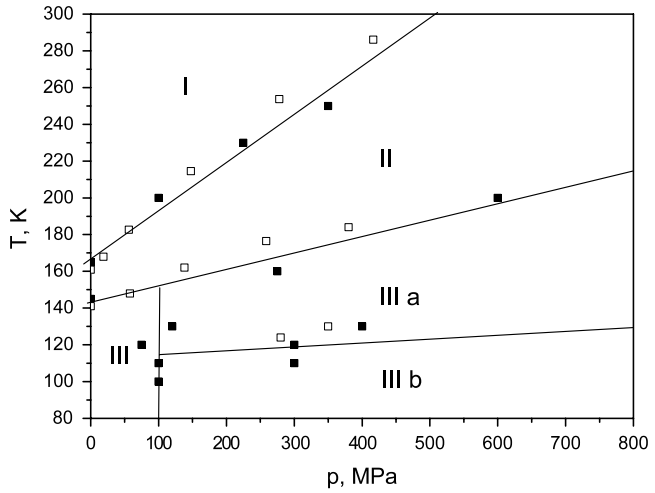

Figure 4. p–T phase diagram of T_2PyHI (□, dielectric spectroscopy; ■, NMR).

anomalies at $T_{\mathrm{I–II}} = 161$ K and $T_{\mathrm{II–III}} = 141$ K and the first one is the Curie point. Under pressure, both anomalies are shifted towards higher temperatures. For pressure higher than 400 MPa the anomalies disappear or become difficult to observe.

The pressure dependences of the spin–lattice relaxation time T_1^H at a few temperatures are presented in figure 3. At 250 K the relaxation time T_1^H increases with increasing pressure and above 375 MPa it begins to decrease. At 160 K the relaxation time T_1^H decreases with pressure increasing up to 275 MPa, and above this pressure it increases. At 130 K the relaxation time T_1^H decreases with pressure increasing up to 120 MPa, and then increases up to 500 MPa, from which it is constant. At 100 K the relaxation time T_1^H starts to increase with increasing pressure and above 100 MPa it reaches a constant value.

The values of temperature and pressure for which a change in the slope (in the sign and/or in the value) of the plot of T_1^H(p) was observed were assumed as the phase transition points. The character of the T_1^H(p) dependence suggests a continuous (second order) or very close to continuous (first order) phase transition.

Figure 4 presents the phase diagram p–T obtained on the basis of the results of dielectric spectroscopy and nuclear magnetic resonance study. With increasing pressure phase III splits into two phases, denoted IIIa and IIIb, so these phases are pressure induced. Moreover, with increasing pressure the temperatures of phase transitions $T_{\mathrm{I–II}}$, $T_{\mathrm{II–IIIa}}$, $T_{\mathrm{IIIa–IIIb}}$ increase. It should be noted that for PyHI the phase transition temperature also increases with increasing pressure [5]. For T_2PyHI the p–T phase diagram shows two triple points of coordinates 150 K, 100 MPa and 115 K, 100 MPa.

The temperature dependence of the elementary cell parameters in the range 110–290 K was obtained on the basis of the single crystal x-ray diffraction study of the monocrystal and is presented in figure 5. The lattice parameters obtained at 24, 100 and 155 K from the neutron diffraction study are also marked in this figure. The phase transition temperatures $T_{\mathrm{I–II}}$ and $T_{\mathrm{II–IIIa}}$ increase linearly with increasing pressure and the slopes of the relevant curves (figure 4) are defined as follows:

$$\mathrm{d}T_{\mathrm{I–II}}/\mathrm{d}p = (40.0 \pm 0.2)\ (\mathrm{K}/(100\ \mathrm{MPa})), \tag{1}$$

$$\mathrm{d}T_{\mathrm{II–IIIa}}/\mathrm{d}p = (18 \pm 2)\ (\mathrm{K}/(100\ \mathrm{MPa})). \tag{2}$$

As indicated by the shapes of the dielectric anomalies and the specific heat anomaly, the phase transition at $T_{\mathrm{I–II}} = 161$ K is continuous, while that at $T_{\mathrm{II–III}} = 141$ K is discontinuous although close to continuous. For the continuous transitions the pressure dependence of the phase transition temperature can be described by the Ehrenfest equation:

$$\mathrm{d}T_{\mathrm{I–II}}/\mathrm{d}p = T^0_{\mathrm{I–II}} * V_{\mathrm{m}} * \Delta\alpha/\Delta C_p, \tag{3}$$

where V_{m} is molar volume, $\Delta\alpha$ the difference in the volume expansion coefficients of the low- and high-temperature phases, and $T^0_{\mathrm{I–II}}$ the phase transition temperature at ambient pressure. For discontinuous transitions the pressure dependence of the phase transition temperature can be described by the Clausius–Clapeyron equation:

$$\mathrm{d}T_{\mathrm{II–III}}/\mathrm{d}p = \Delta V_{\mathrm{m}}/\Delta S, \tag{4}$$

where ΔV_{m} is the change in the molar volume and ΔS is the change in entropy accompanying the first order transition.

The application of the Ehrenfest and Clausius–Clapeyron equations requires the measurements of the specific heat and temperature dependence of the crystal volume. Specific heat was measured by the DSC method [2], while the temperature dependence of the crystal volume was derived from the x-ray measurements of the lattice constants (figure 5). The following parameters of the Ehrenfest equation were obtained:

$\alpha_{\mathrm{II}} = 0.637 \times 10^{-4}$ (K^{-1})—volume expansion coefficient of phase II,

$\alpha_{\mathrm{I}} = 4.130 \times 10^{-4}$ (K^{-1})—volume expansion coefficient of phase I,

$\Delta\alpha = \alpha_{\mathrm{II}} - \alpha_{\mathrm{I}} = 3.493 \times 10^{-4}$ (K^{-1})—difference in the volume expansion coefficients,

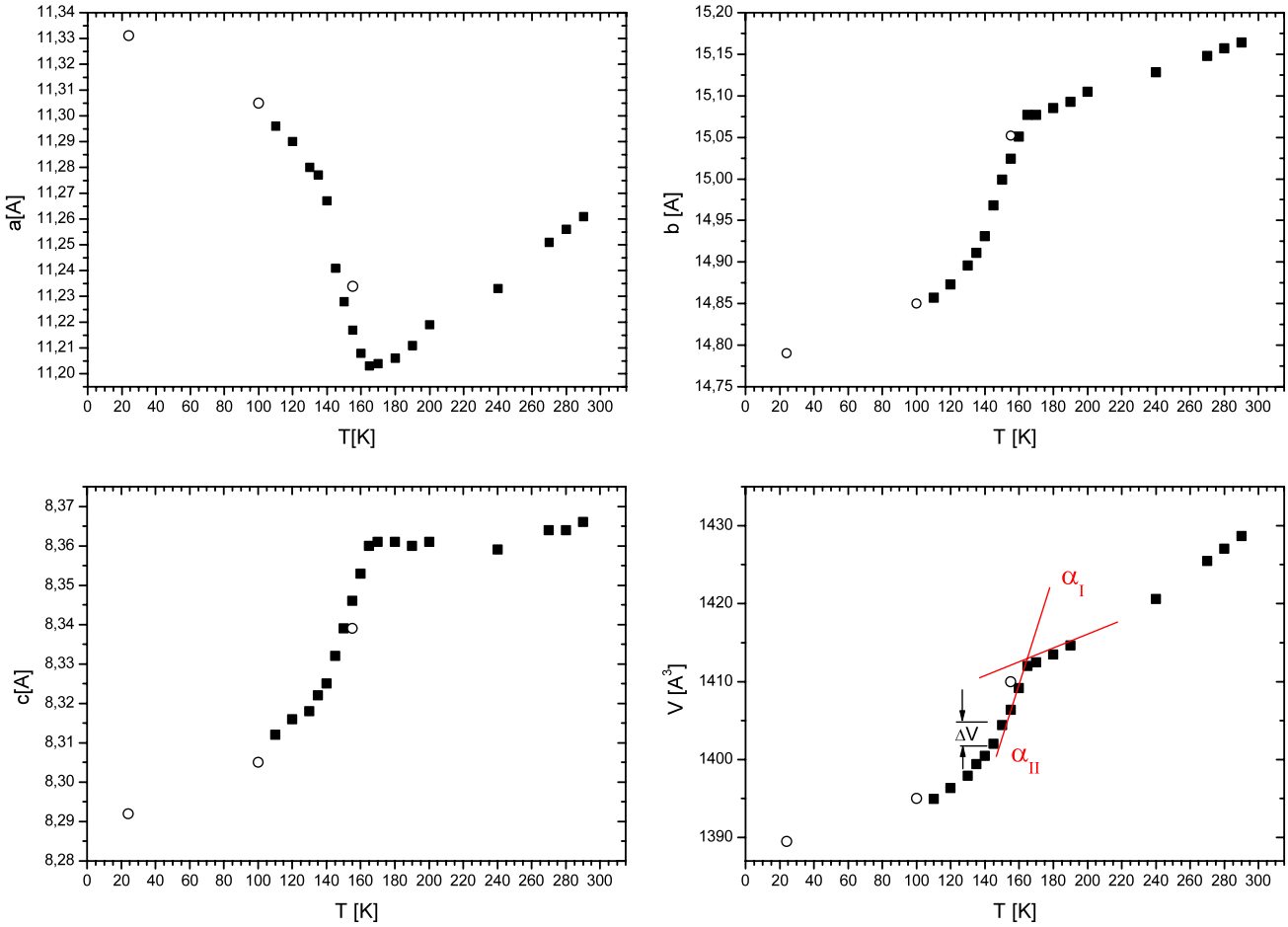

Figure 5. The temperature dependence of the volume and elementary cell parameters (■, single crystal x-ray diffraction; ○, neutron diffraction).

$\Delta C_p = 29.7 \pm 0.2$ (J mol^{-1} K^{-1})—change in the specific heat at $T_{\mathrm{I–II}} = 161$ K,

$V_{\mathrm{m}} = 211.3 \times 10^{-6}$ (m^3 mol^{-1}) (density $\rho = 1.702$ g cm^{-3}, molar mass = 359.25 g),

$T^0_{\mathrm{I–II}} = 161$ (K)—phase transition temperature at ambient pressure.

Using the above parameters, the Ehrenfest equation gives $\mathrm{d}T_{\mathrm{I–II}}/\mathrm{d}p = 39.7$ (K/(100 MPa)).

This value $\mathrm{d}T_{\mathrm{I–II}}/\mathrm{d}p = 39.7$ is in a very good agreement with the coefficient of equation (1) for the continuous phase transition at $T_{\mathrm{I–II}}$.

A calculation of $\mathrm{d}T_{\mathrm{II–III}}/\mathrm{d}p$ for the phase transition at $T_{\mathrm{II–III}}$ requires the use of the Clausius–Clapeyron equation (4). Of key importance is the precise determination of the difference in the volume ΔV at $T_{\mathrm{II–III}}$ and the change in entropy ΔS. Unfortunately, this difference is poorly visible in figure 5 ($\Delta V \sim 2.5$ (Å^3) which is $\Delta V_{\mathrm{m}} \sim 0.39 \times 10^{-6}$ (m^3 mol^{-1})) and its estimated value is charged with great error. The parameters of the Clausius–Clapeyron equation are

$$\Delta V_{\mathrm{m}} = (0.39 \pm 0.08) \times 10^{-6} \text{ (m}^3 \text{ mol}^{-1}\text{)},$$

$$\Delta S = (3.4 \pm 0.3) \text{ (J mol}^{-1} \text{ K}^{-1}\text{)}.$$

From equation (4), $\mathrm{d}T_{\mathrm{II–III}}/\mathrm{d}p = 12 \pm 4$ (K/(100 MPa)). Taking into regard the accuracy of the fit of equation (2) and the accuracy of the estimation of $\mathrm{d}T_{\mathrm{II–III}}/\mathrm{d}p$ from equation (4), the results obtained (18±2) (K/(100 MPa)) and $\mathrm{d}T_{\mathrm{II–III}}/\mathrm{d}p = 12 \pm 4$ (K/(100 MPa)) could be assumed to be satisfactory.

4. Neutron scattering

The neutron diffraction spectra were recorded at normal pressure and at 24, 100, 155 and 190 K (figure 6). The diffraction peaks were indexed according to the structural data presented in [2]. Unlike the phase transition from II to I, which is not observed in the neutron spectra, the phase transition from III to II ($T_{\mathrm{III–II}} = 141$ K) is clearly visible. In order to verify the presence of the pressure-induced phases, neutron diffraction measurements were performed under varying pressure. At 100 K the neutron diffraction measurements were made at the pressures 0.1, 95, 215 and 300 MPa (figure 6). The neutron powder diffraction spectra recorded as a function of pressure are of poorer quality than those recorded as a function of temperature due to the thick-walled pressure chamber. The background coming from the pressure chamber is present as well; see figure 6. The neutron powder diffraction spectra measured at 100 K at normal pressure and 95 MPa differ from

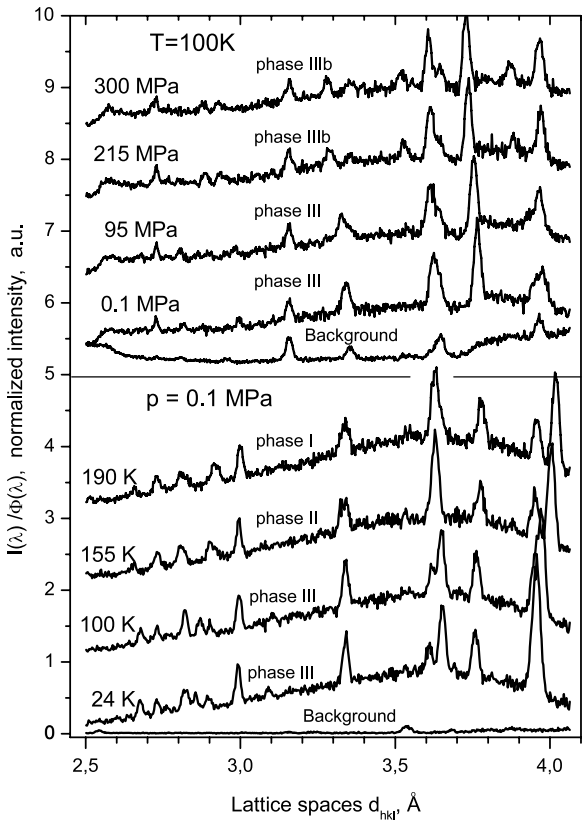

Figure 6. The neutron diffraction spectra as a function of temperature (top) and pressure (bottom), $2\theta = 118°$.

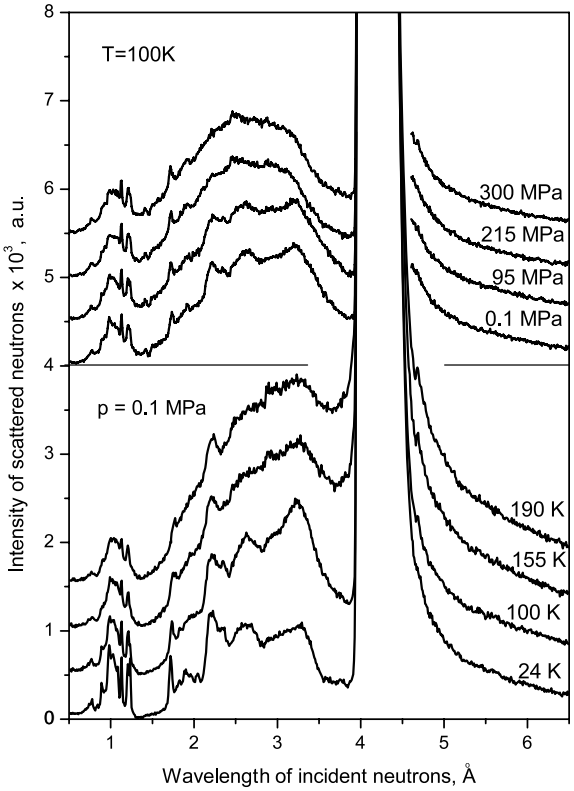

Figure 7. The temperature (bottom) and pressure (top) dependences of the IINS spectra as a function of the wavelength of the incident neutrons.

those recorded at 215 and 300 MPa, which proves the presence of a new pressure-induced phase IIIb. The diffraction spectra in the new phase do not have a sufficient number of peaks to determine a space group on its basis.

Figure 7 presents the inelastic incoherent neutron scattering (IINS) spectra measured at different temperatures at normal pressure and at 100 K at different pressures, which correspond to the conditions in which the neutron powder diffraction spectra were reordered (see figure 6). The effect of the high-pressure chamber can be seen by comparing the IINS spectra measured at 100 K and at ambient pressure. The $T_{\mathrm{II–III}} = 141$ K phase transition is reflected by the appearance of the quasielastic (QENS) wings of the elastic line at 4.25 Å and the broadening of the low frequency inelastic bands seen at 2.5 and 3.3 Å. The pressure dependence of the IINS spectra at 100 K indicates a new phase IIIb at 215 and 300 MPa. In this case the lowest frequency band seen at 3.3 Å is shifted to the higher frequencies and mixed with other phonon branches seen at 2.2 and 2.6 Å. In consequence, a structure of these phonon branches disappears in the IINS spectrum of phase IIIb. The high frequency cut-off of the lattice modes in the IINS spectra is seen at the 1.7 Å wavelengths of incoming neutrons. No mixing between the lattice and internal vibrations takes place. The energy gap between these vibrations is in the range of wavelengths from 1.3 to 1.6 Å. The internal vibrations do not undergo a significant modification in pressure and temperature changes, except the band broadening with increasing temperature.

For more detailed analysis the IINS spectra were converted to the generalized phonon density of states $G(\omega)$, in the one-phonon scattering approximation [22, 23]. The corresponding $G(\omega)$ functions in the frequency range up to 200 cm^{-1} are shown in figure 8. The $G(\omega)$ spectra obtained at 0.1 and 95 MPa are very similar and reveal a maximum at the frequency of 28 cm^{-1}, assigned to the low frequency librations. The $G(\omega)$ spectra at 215 and 300 MPa are also similar but do not show a maximum in the low frequency region. Our interpretation is that this low frequency libration band was shifted towards higher frequency with increasing pressure. As a result of hybridization of the lattice vibrations with this vibration the dispersion of lattice vibrations increased, which resulted in smoothing the $G(\omega)$ spectrum recorded at 215 and 300 MPa. Such behaviour of the phonon density of states function confirms the occurrence of the phase transition from phase III to IIIb. In the frequency range up to 200 cm^{-1}, the $G(\omega)$ function shows maxima at 60, 96, 140 and 180 cm^{-1}. The band with a maximum at 180 cm^{-1} (at normal pressure) is slightly shifted towards higher frequencies with increasing pressure but its width does not change at the phase transition. This means that the highest frequency phonon branch does not mix with other phonon branches and has a low dispersion.

Figure 8 presents $G(\omega)$ spectra obtained at 24, 100, 155 and 190 K for normal pressure. Similarly as for the above pressure dependence of $G(\omega)$, the spectra for the temperatures 24 and 100 K are very

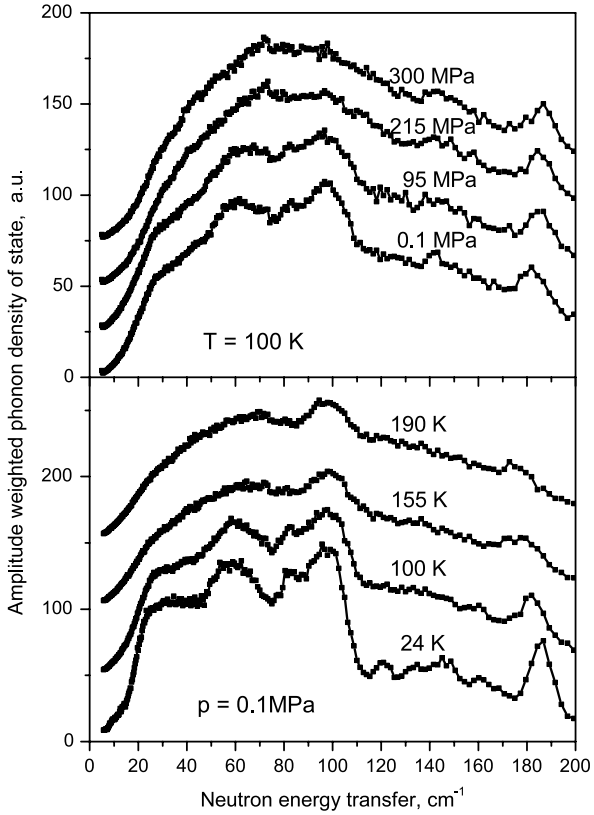

Figure 8. The temperature (bottom) and pressure (top) dependences of the amplitude weighted phonon density of states—$G(\omega)$ spectra.

similar and show the low frequency band at 28 cm^{-1}. The $G(\omega)$ spectra obtained for 155 and 190 K do not show any maximum in the low frequency region. We suppose that this low frequency libration band is overdamped above the temperature of the $T_{II–III} = 141$ K phase transition. At 155 K (phase II) and 190 K (phase I) QENS broadening has appeared as a result of stochastic jumps of the pyridinium cation. The band with a maximum at 180 cm^{-1} (as recorded at 24 K) with increasing temperature is shifted towards lower frequencies and its width undergoes a jump change at the $T_{II–III} = 141$ K phase transition.

Figure 9 presents the spectral density functions $G(\omega)$ (up to 1000 cm^{-1}) for PyHI, thiourea, and T_2PyHI, obtained from the IINS spectra recorded at 24 K. For all these compounds the energy gap between the lattice and internal vibrations is in the same energy range from 200 to 400 cm^{-1}. The $G(\omega)$ functions for these compounds differ for the lattice vibrations and for the internal vibrations; however, the lowest frequency of internal modes has a very similar value of 415 cm^{-1}. Most probably, the increasing pressure causes a deformation of the channels formed by the thiourea molecules and iodide anions. It leads to a modification of the dynamics of the lattice of the system studied and the dynamics of the pyridinium cations placed in the channels. The next stage of the study will be a determination of the structures of the pressure-induced phases (IIIa and IIIb) by the neutron diffraction method performed for a polycrystalline sample. We wish to study the effect of pressure on the dynamics of the pyridinium cations.

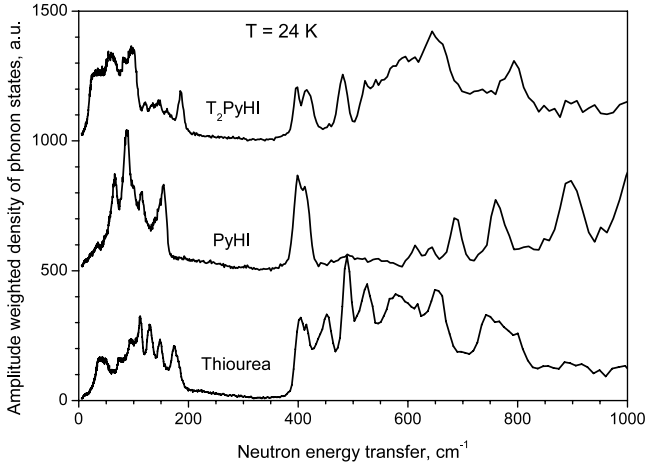

Figure 9. The amplitude weighted phonon density of states—$G(\omega)$ spectra for PyHI, thiourea and T_2PyHI at 24 K.

5. Conclusions

(1) The results obtained by dielectric spectroscopy, neutron diffraction and NMR study permitted a construction of the p–T phase diagram for T_2PyHI.

(2) The temperatures of phase transitions $T_{I–II}$, $T_{II–IIIa}$, $T_{IIIa–IIIb}$ are shifted towards higher values with increasing pressure. The shapes of the dielectric anomalies and the specific heat anomaly indicate that the phase transition at $T_{I–II} = 161$ K is continuous, while the one at $T_{II–III} = 141$ K is discontinuous or discontinuous but close to continuous.

(3) The results have shown the occurrence of two new high-pressure phases with triple points of coordinates 150 K, 100 MPa and 115 K, 100 MPa.

Acknowledgment

The work has been partially financed by the Ministry of Science and Higher Education of Poland from 2006–2008 funds, grant no N202 134 31/2331.

References

[1] Małuszyńska H and Czarnecki P 2006 *Z. Kristallogr.* **221** 218
[2] Małuszynska H, Czarnecki P, Fojud Z and Wąsicki J 2008 *Acta Crystallogr.* B **64** 567
[3] Prout K, Heyes S J, Dobson Ch M, McDaid A, Maris T, Müller M and Seaman M J 2000 *Chem. Mater.* **12** 3561
[4] Ripmeester J 1986 *J. Chem. Phys.* **85** 747
[5] Lewicki S, Wąsicki J, Czarnecki P, Szafraniak I, Kozak A and Pająk Z 1998 *Mol. Phys.* **94** 973
[6] Wąsicki J, Nawrocik W, Pająk Z, Natkaniec I and Belushkin A V 1989 *Phys. Status Solidi* a **114** 497
[7] Mukhopadhyay R, Mitras S, Tsukushi I and Ikeda S 2001 *Chem. Phys. Lett.* **341** 45
[8] Czarnecki P, Nawrocik W, Pająk Z and Wąsicki J 1994 *Phys. Rev.* B **49** 1511
[9] Czarnecki P, Nawrocik W, Pająk Z and Wąsicki J 1994 *J. Phys.: Condens. Matter* **6** 4955

[10] Wąsicki J, Czarnecki P, Pająk Z, Nawrocik W and Szczepański W 1997 *J. Chem. Phys.* **107** 576
[11] Pająk Z, Czarnecki P, Wąsicki J and Nawrocik W 1998 *J. Chem. Phys.* **109** 6420
[12] Pająk Z, Małuszyńska H, Szafrańska B and Czarnecki P 2002 *J. Chem. Phys.* **117** 5303
[13] Pająk Z, Czarnecki P, Małuszyńska H, Szafrańska B and Szafran M 2000 *J. Chem. Phys.* **113** 848
[14] Fojud Z, Goc R, Jurga S, Kozak A and Wąsicki J 2003 *Mol. Phys.* **101** 1469
[15] Beck B, Villanueva-Garibay J A, Muller K and Roduner E 2003 *Chem. Mater.* **15** 173
[16] Vujosevic D, Muller K and Roduner E 2006 *J. Phys. Chem.* B **110** 8598
[17] Wąsicki J, Fojud Z, Czarnecki P and Jurga S 2008 *Ferroelectrics* at press
[18] Wąsicki J, Pajzderska A and Fojud Z 2008 *J. Phys. Chem.* C **112** 7503
[19] Grottel M, Pajzderska A and Wąsicki J 2003 *Z. Naturf.* a **58** 638
[20] Natkaniec I, Bragin S I, Brankowski J and Mayer J 1994 *Proc. ICANS-XII (Abingdon 1993) RAL Report 94-025* vol I, p 89
[21] Habrylo S, Bragin S I, Brankowski J, Iwanski W, Mayer J, Natkaniec I, Nawrocik W and Zawalski K 1990 *High Pressure Res.* **4** 457
[22] Gurevich I I and Tarasov L V 1965 *Physics of Low Energy Neutrons* (Moscow: Nauka)
[23] Pokotilovski Yu N, Natkaniec I and Hołderna-Natkaniec K 2008 *Physica* B **403** 1942